A 1.5D fluid - Monte Carlo model of a hydrogen helicon plasma

R. Agnello,[1] G. Fubiani,[2] I. Furno,[1] Ph. Guittienne,[1] A. Howling,[1] R. Jacquier,[1] and F. Taccogna[3]
[1)]*École Polytechnique Fédérale de Lausanne (EPFL), Swiss Plasma Center (SPC), CH-1015 Lausanne, Switzerland*
[2)]*LAPLACE, Université de Toulouse, CNRS, INPR, UPS, France*
[3)]*Istituto di Metodologie Inorganiche e dei Plasmi-CNR, via Amendola 122/D, 70126 Bari, Italy*

Helicon plasma sources operating with hydrogen or deuterium might be attractive for fusion applications due to their higher power efficiency compared to inductive radiofrequency plasma sources. During recent years, the Resonant Antenna Ion Device (RAID) has been investigating the physics of helicon plasmas and the possibility of employing them to produce negative ions for Heating Neutral Beam injectors (HNBs). We present herein a fluid-Monte Carlo model describing plasma species transport of a typical helicon hydrogen plasma discharge. This work is motivated by the interest to better understand the basic physics of helicon plasma devices when operating in hydrogen and, in particular, the volume production of negative ions. This model is based on the synergy between two separately self-consistent approaches: a plasma fluid model calculating ion transport, and a Monte Carlo (MC) model, to determine neutral and rovibrational density profiles of H_2. By introducing as model constraints the electron density and temperature profiles measured by Langmuir Probes, the densities of ion species (H^+, H_2^+ , H_3^+, H^-) are computed in a 1.5D (dimensional) geometry. The estimate of the negative ion density profile represents a useful benchmark to be compared with dedicated diagnostics such as Cavity Ring-Down Spectroscopy and Langmuir probe laser photodetachment. Neutral gas particles (atoms and molecules) are calculated assuming a fixed plasma background. This gas-plasma decoupling is necessary due to the different timescales of plasma (microseconds) and gas kinetics (milliseconds).

I. INTRODUCTION

The fusion reactor ITER will be equipped with two Heating Neutral Beam injectors (HNB) to heat up the plasma to the required conditions for controlled nuclear fusion.[1] To produce high energy (up to 1 MeV) atomic beams, negative ions (H^- or D^-) are accelerated and then neutralized by charge exchange with a background gas along the beam propagation direction. Negative hydrogen and deuterium ions for HNB applications are routinely produced in large plasma sources such as SPIDER[2] and ELISE[3], by means of radiofrequency inductive plasma sources. The comprehension of the physics mechanisms describing the transport and extraction of negative hydrogen and deuterium ions in these sources is supported by numerical simulations.[4,5] Low pressure hydrogen and deuterium plasmas are composed of different ionic and gas species including positive and negative ions, ground state atoms and molecules, atomic and molecular electronic excited states, molecular rovibrational states and radicals.
In recent years, the possibility to produce negative ions (H^- or D^-) for HNB injectors by means of helicon plasma sources was investigated at the Resonant Antenna Ion Device (RAID) experiment.[6,7] In parallel, other helicon plasma sources operate worldwide to study the volume production of negative ions in helicon-sustained plasmas.[8–11] In RAID, plasmas are sustained by a resonant birdcage antenna used as a helicon plasma source[12] up to 10 kW long-pulse operation. Numerical simulations are underway to investigate the physics of helicon waves[13] and plasma transport[14] in RAID for typical H/D plasma discharges. As part of the numerical simulation efforts and cross check with experimental data, we present herein a 1.5D fluid - MonteCarlo (MC) model aimed to the description of the transport of plasma and neutral species of a typical hydrogen helicon plasma produced in RAID. As "1.5D" model we intend that it describes the dynamic along the radial direction while retaining some axial physics. In particular, ion losses along the direction of the magnetic field are considered. The 1.5D geometry for RAID is justified by the cylindrical symmetry in density and temperature of helicon plasmas and their uniformity along the plasma column axis.
Fluid models can be employed to understand the physical principles of certain magnetized plasmas, in particular they can very successful in low pressure, low beta plasmas which are relatively more stable. Advanced 2D and 3D models, required by the lack of particular symmetries, are currently used to describe plasmas produced by inductive plasma sources for HNB injectors.[15] Fluid models have been employed to describe highly collisional plasmas, such as on the edge of fusion plasmas, small toroidal experiments (TORPEX) and steady state linear plasma devices.[16] Unlike other helicon linear reactors where the plasma is bounded by long and narrow dielectric tubes, RAID vessel walls are far from the edge of the plasma column and electrically conducting. This suggests that boundary conditions are mainly dominated by endplates on which important plasma losses and recombination processes occur. A comprehensive description of a hydrogen helicon discharge would require coupling the helicon wave propagation and power deposition mechanisms to a transport/chemistry model. This is beyond the scope of the present work, aimed at investigating the role of plasma reactions and species profiles, which cannot be easily separately measured.
The paper is structured as follows. In Sec. II, the RAID device and its parameters are presented. In Sec. III, the equations of the fluid model are discussed, as well as the plasma chemistry and the model inputs. In Sec. IV, the MC model for neutral particles is described. In Sec. V, the output data of the model are presented including plasma species profiles, source profiles, generation/loss mechanisms for H^- and comparison with experimental measurements. In Sec. VI, we discuss conclusions and possible applications of this model.

II. EXPERIMENTAL SETUP AND PARAMETERS

Plasma discharges in the RAID device are excited by a radiofrequency (RF) antenna in a birdcage geometry able to sustain the propagation of helicon waves.[12] The antenna is wrapped around a ceramic cylinder with external diameter 11.5 cm, internal diameter 9.5 cm and 38 cm long mounted on one end of a stainless steel cylindrical vessel 1.5 m long and 40 cm diameter and can deliver up to 10 kW to the plasma. A set of 6 coils generates a DC magnetic field along the axis up to 800 mT. Further details on RAID can be found in other works.[6,7,17]

The fluid model can be applied provided that the ion-neutral collision mean free path (mfp) is smaller than the typical size of the device. Tab. I summarizes RAID typical hydrogen plasma and device parameters. Similarly to hot fusion plasmas, the magnetic field can play an important role in plasma transport in low-pressure plasma sources.[5] The typical values of RAID magnetic field (0.01 - 0.1 T) are such that the ion and electron Larmor radii are in the sub millimeter range, therefore the plasma is strongly magnetized and charged particles are constrained to flow along the magnetic field lines. Cross field diffusion is however possible due to particle collisions producing displacements along the radial direction, whose size is of the order of the Larmor radius. Along the axial direction, charged particles freely stream and undergo collisions with the background gas (H_2) with a mfp of the order of 0.1 m, shorter than the plasma axial length (1.8 m). The degree of anisotropy in the ion transport is such that the typical ratio between axial and perpendicular diffusion coefficient is:[18]

$$D_\parallel / D_\perp = 1 + \left(\frac{\omega_c}{\nu}\right)^2 \approx 10^2 - 10^3, \tag{1}$$

where ω_c is the ion cyclotron frequency and ν the typical ion-gas collision frequency.

The RAID vessel is supplied with a H_2 flow rate of 10 sccm and constant pressure of 0.3 Pa, corresponding to a molecular density of $7.25 \times 10^{19}\mathrm{m}^{-3}$ at room temperature (300 K). Given the typical plasma density generated in the center of a hydrogen plasma column ($2.5 \times 10^{18}\mathrm{m}^{-3}$), we make the assumption that plasma species are diluted in a H_2 background. Ion transport can then be described by classical drift-diffusion equations in the presence of a uniform magnetic field. At this low RF power ($\lesssim 5\,\mathrm{kW}$) and gas pressure ($p \lesssim 1\,\mathrm{Pa}$) neutral depletion,[19] consisting in the displacement of neutrals to the walls of the device at high plasma densities ($\gtrsim 10^{19}\,\mathrm{m}^{-3}$), can be neglected. As far as it concerns coulomb collisions, in the case of like-particles (electron-electron and ion-ion collisions), these do not cause diffusion.[20] Only electron-ion collisions might play a role. Electron-ion collision frequency is about one order of magnitude larger than the electron-neutral collision frequency, however, due to large mass difference, the relative momentum exchange is of the order of $\Delta p/p \approx \sqrt{(m_e/m_i)}\sqrt{(T_e/T_i)} \approx 0.15$, therefore, Coulomb collisions should not affect considerably the ion diffusion with respect to the background neutral gas. Plasma instability and turbulence might occur in a mid/high power helicon plasma device such as RAID and would require to take into account non linear terms, dramatically complicating the model. However, as we will see later on, RAID plasma is well described by classical diffusion in a magnetic field, so we do not take into account non-linear phenomena in a first-order modeling.

Parameter	Value
Vessel Radius	0.2 m
Gas pressure	0.15 - 1.5 Pa
Magnetic field	0.01 - 0.1 T
Plasma axial length	1.8 m
Plasma density	$\lesssim 2 \times 10^{18}\,\mathrm{m}^{-3}$
Electron temperature	$\lesssim 8\,\mathrm{eV}$
Ion temperature	$\lesssim 0.1\mathrm{eV}$
Ion cyclotron frequency	$3.05 \times 10^5\,\mathrm{s}^{-1}$ ($B = 20\,\mathrm{mT}$)
Electron cyclotron frequency	$5.6 \times 10^8\,\mathrm{s}^{-1}$ ($B = 20\,\mathrm{mT}$)
H_2^+-H_2 collision frequency	$2.36 \times 10^4\,\mathrm{s}^{-1}$
Electron-H_2 collision frequency	$1.19 \times 10^5\,\mathrm{s}^{-1}$
Electron-H_2^+ collision frequency	$2.5 \times 10^6\,\mathrm{s}^{-1}$
Electron-electron collision frequency	$6.25 \times 10^6\,\mathrm{s}^{-1}$
H_2^+-H_2^+ collision frequency	$2.61 \times 10^7\,\mathrm{s}^{-1}$
H_2^+-H_2 mean free path	$\approx 0.1\,\mathrm{m}$
electron-H_2^+ mean free path	$\approx 5\,\mathrm{mm}$
Ion Larmor radius	$\lesssim 1\,\mathrm{mm}$
Electron Larmor radius	$\lesssim 0.25\,\mathrm{mm}$
Debye length	$\approx 10^{-5}\,\mathrm{m}$

TABLE I: Typical parameters for a hydrogen plasma discharge in RAID. The size of the ion Larmor radius, compared to the size of the vessel, makes it possible to describe the ion transport with a fluid model.

III. DESCRIPTION OF THE MODEL

A. Basic equations

The equations composing the fluid description are the continuity, the momentum and the Poisson equations, which are written below. Each ion species is denoted by the subscript s, where s can be H^+, H_2^+, H_3^+ or H^-. The continuity and the ion momentum conservation equations are:

$$\frac{\partial n_s}{\partial t} + \nabla \cdot \vec{\Gamma}_s = S_s - L_s, \tag{2}$$

$$m_s n_s \left[\frac{\partial \vec{u}_s}{\partial t} + (\vec{u}_s \cdot \nabla)\vec{u}_s\right] = q_s n_s (\vec{E} + \vec{u}_s \times \vec{B}) - \nabla \cdot \bar{\bar{P}}_s - m_s n_s \nu_s \vec{u}_s, \tag{3}$$

where n_s is the number density, m_s the mass, $\vec{u}_s$ the fluid velocity of the species, $\vec{E}$ the electric field, $\vec{B}$ the magnetic field, $\bar{\bar{P}}_s$ the partial pressure tensor (due to ions only), q_s the electron charge magnitude, $\vec{\Gamma}_s = n_s \vec{u}_s$ the flux of species, ν_s the momentum transfer frequency and S_s and L_s the source and the loss terms.

The electric field and the plasma potential V are calculated using the Poisson equation:

$$\nabla^2 V = -\frac{e}{\varepsilon_0}(n_{H^+} + n_{H_2^+} + n_{H_3^+} - n_{H^-} - n_e), \tag{4}$$

with

$$\vec{E} = -\nabla V, \tag{5}$$

where n_e is the electron density and ε_0 is the vacuum dielectric constant. Plasma quasi-neutrality is guaranteed by the electric field generated by the charge separation. Due to the cylindrical symmetry of the RAID plasma, the magnetic DC field as well as the electric field generated by the plasma potential have no azimuthal components. However they produce a $\vec{E} \times \vec{B}$ and a diamagnetic drift along the azimuthal direction of the charged fluids with associated tangential fluxes. If we consider axial invariance, the total flux can be expressed as the sum of a radial and an azimuthal component, namely $\vec{\Gamma} = \vec{\Gamma}_r + \vec{\Gamma}_\phi$. Equations (2), (3) and (4) are then solved with the PDE (partial differential equation) module of the finite element calculator COMSOL multiphysics.[21]

Assuming cylindrical symmetry of the plasma discharge, the continuity equation can be written as:

$$\frac{1}{r}\frac{\partial(r\Gamma_r)}{\partial r} = S(r) - 2\frac{\Gamma_z(r)}{L_z}, \tag{6}$$

where $S(r)$ is the source term of any species along the radial direction (it takes into account the sum of sources and losses in volume), and $2\frac{\Gamma_z(r)}{L_z}$ is the term describing the particle losses along the axial direction z due to the free streaming along the magnetic field lines up to both endplates. Due to this term we define the model to have a 1.5D geometry. $\Gamma_z(r)$ is the flux of particles at the discharge ends at radius r. For positive ions $\Gamma_z(r)$ reads:

$$\Gamma_z(r) = \alpha n_s u_{Bohm}(r), \tag{7}$$

where u_{Bohm} is the Bohm velocity $u_{Bohm,s} = \sqrt{q_s T_e / m_s}$. α is a factor dependent on the presheath voltage drop and depends on the conditions in the collisional presheath, particularly on the plasma flow velocity and electron and ion temperatures. The presheath drop dictates what the density at the sheath would be.

From Eq. (3) one can derive the expression for the radial flux; for positive ions this reads:

$$\Gamma_r = \frac{q_s \nu_s n_s}{m_s(\nu_s^2 + \omega_{c,s}^2)}\left(E_r - \frac{T_s}{n_s}\frac{dn_s}{dr}\right), \tag{8}$$

where $\omega_{c,s} = \frac{q_s B}{m_s}$ is the ion cyclotron frequency.

B. Assumptions

It is useful to summarize in this paragraph the main simplifying assumptions.
We neglect the acceleration term, $\frac{\partial \vec{u}_s}{\partial t}$, since we assume to be in steady state regime. For the ion inertia term, $(\vec{u}_s \cdot \nabla)\vec{u}_s$, we assume that diffusive time scale are much slower than bulk flow time scales.[18] The inclusion of the inertial term would lead to the separation of the momentum equation in each dimension for each species increasing the complexity of the model.[22]
The ion distribution function is considered isotropic and, also, we neglect the gradient of the ion temperature (we assume 0.1 eV uniform ion temperature and the same for all ion species), therefore $\nabla \cdot \bar{\bar{P}}_s = k_b T_s \nabla n_s$, where k_b is the Boltzmann's constant.
The magnetic field $\vec{B}$ takes into account only the DC field generated by the external coils (200 mT) since the magnetic field generated by plasma currents is negligible (the magnetic field of the helicon wave is a few Gauss[13]).
The magnetic pressure is significantly larger than plasma pressure, rendering all plasma diamagnetic effects negligible. The ratio between the plasma kinetic pressure and the plasma magnetic pressure provides:

$$\frac{p_{magnetic}}{p_{plasma}} = \frac{B^2/2\mu_0}{k_b n_e T_e} \approx 100 \tag{9}$$

C. Boundary conditions

The vessel walls and endplates play an important role in the plasma equilibrium. They govern the rate at which particles are lost from the plasma bulk as well as the surface chemistry. This is particularly relevant in the case of a linear plasma device, such as RAID, where magnetic field lines intersect the boundaries of the device. In the literature, authors have investigated the effect of changing the position and the electric properties of the endplates,[23] which have an effect on the axial boundary conditions of the helicon wave and in turn on the discharge properties.
A rigorous description of wall losses would require a self consistent treatment of the plasma sheath. In the sheath region (a few mm in front of the wall) the quasi-neutrality is lost and therefore strong electric fields appear. From the modeling point of view, this would imply strong charged particles accelerations and problems of numerical convergence. To accurately resolve the dynamics of the ion free fall across the plasma sheath, one should locally redefine the meshing with at least a sub millimetric resolution. The coupling of the bulk plasma region with the plasma sheath region would require to considerably increase the complexity of the transport model without adding any particular relevant element to the overall transport dynamic and chemistry. Therefore, the ion losses at the boundaries are estimated according to the Bohm expression, which for positive ions reads:

$$\Gamma_{wall} = -\sqrt{(qT_e/m_s)}n_s e^{-\frac{1}{2}}. \tag{10}$$

Negative ions (such as H^-), due to their negative charge, are confined in the plasma bulk, in electropositive plasmas.[24] The typical temperature of ions in low temperature plasma devices ($\sim 0.1\,\mathrm{eV}$) is indeed insufficient to overcome the plasma potential well. H^- ions are therefore produced and destroyed in the plasma volume. In a volume negative ion source like RAID, it is therefore crucial to understand the interplay between production and destruction channels of negative ions, discussed in Sec. V B, and how they can be controlled to optimize negative ion yield.

D. Reaction rates

In this model, we consider volume reactions between electrons and neutral/ion species, between atomic and ion species and between ion species in the plasma bulk. We do not consider three body reactions, since they are negligible at this low pressure regime. The reaction rate R is given by the product of the densities n_1 and n_2 of the reactants and is regulated by a rate coefficient $k(T_1,T_2)$, dependent on the reactants' temperature T_1 and T_2:

$$R = k(T_1,T_2)n_1n_2 \quad [\mathrm{m^{-3}s^{-1}}]. \tag{11}$$

To describe the chemistry of the hydrogen plasma discharge in RAID, we have employed the reaction set in Tab. II, which shows the complexity of the plasma chemistry in this model.

For reaction 3, we have employed the dissociative attachment reaction rate provided in Ref.[25], whereas, for the others, we have employed the reaction rates provided in Ref.[22]. The channels for the volume production of H^- are given by reactions 3, 7 and 22. We will see that reaction 3, the dissociative attachment, is by far the most effective channel for H^- production in the plasma. The net source term for each ion species is reported in the set of Eqs. 12.

$$\begin{cases} \nabla\cdot\Gamma_{H^+} &= k_4n_en_H + k_5n_Hn_{H^+} + k_6n_en_{H_2^+} - k_9n_{H^+}n_{H^-} + k_{13}n_en_{H_3^+} - k_{14}n_{H_2}n_H - k_{21}n_{H_2}n_{H^+}, \\ \nabla\cdot\Gamma_{H_2^+} &= k_{11}n_en_{H_2} - k_5n_Hn_{H_2^+} - k_6n_en_{H_2^+} + k_7n_en_{H_3^+} - k_8n_{H_2}n_{H_2^+} - k_{10}n_{H_2^+}n_{H^-} - k_{15}n_en_{H_2^+} + k_{21}n_{H_2}n_{H^+}, \\ \nabla\cdot\Gamma_{H_3^+} &= -k_7n_en_{H_3^+} + k_8n_{H_2}n_{H_2^+} - k_{11}n_{H_3^+}n_{H^-} - k_{13}n_en_{H_3^+} + k_{14}n_{H_2}n_{H^+} - k_{16}n_en_{H_3^+} - k_{17}n_en_{H_3^+}, \\ \nabla\cdot\Gamma_{H^-} &= n_e\sum_{v=0}^{14}k_3(v)n_{H_2(v)} + k_7n_en_{H_3^+} - k_9n_{H^+}n_{H^-} - k_{10}n_{H_2^+}n_{H^-} - k_{11}n_{H_3^+}n_{H^-} - k_{12}n_en_{H^-} + \\ & \quad -k_{18}n_Hn_{H^-} - k_{19}n_{H_2}n_{H^-} - k_{20}n_Hn_{H^-} + k_{22}n_en_H. \end{cases} \tag{12}$$

The generation rate of H^- by dissociative attachment from ro-vibrationally excited H_2, which is the term $\sum_{v=0}^{14}k_3(v)n_{H_2(v)}$, is calculated by taking into account the density of H_2 molecules in each vibrational state v, computed by the MC model (see Sec. IV). The most important H^- destruction processes are the mutual neutralisation (MN) with positive ions (R9-11), the electron detachment (ED) (R12) and the associative detachment (AD) with neutrals (R18-20).

E. Structure of the model

A complete fluid model describing all species would require the inclusion of a balance equation for electrons and an equation for the power deposition. In RAID, the electron temperature and density profiles can be measured by Langmuir probes and microwave interferometry across the entire volume of the device.[4] These data are introduced as a physical constraint on the basis of which transport and chemistry of the other ion species and atomic hydrogen can be computed. A typical electron density and temperature profile at 1 m from the center of the antenna, 3 kW RF power and 0.3 Pa of gas pressure is shown in Fig. 1, and will be taken as input profile for the modeling. Fig. 2 provides a diagram description of the structure of the model.

F. Dissociative attachment reactions

In plasma, molecular hydrogen can be rovibrationally excited by electron impact or by decay from the excited molecule, sustaining 15 vibrational states in the electronic ground state. Experimental and theoretical studies have revealed that dissociative attachment to these vibrationally-excited states is the main mechanism responsible for volume production of negative ions.[27] A detailed description of the overall hydrogen plasma transport would require the inclusion of reactions involving the collisions between H_2 in the various vibrational states and other plasma species and the respective transport equations. This would increase the number of possible reactions to a few hundreds, increasing the complexity of the model, without substantially changing the transport of ion species. Indeed, since for RAID plasma regime we expect a small amount of excited H_2 (of the order of 1% compared to background H_2[4]), the overall transport and chemistry of ions are expected to be weakly influenced by the presence of excited H_2. To approximate the contribution of the dissociative attachment to H^- production, the MAR (molecular activated recombination) rate coefficient could be used

	Reaction	Reaction Rate (k_n) [m^3s^{-1}]
1	$e + H_2 \rightarrow H_2^+ + 2e$	$7.27 \cdot 10^{-15} T_e^{0.549} e^{-15.5/(T_e-0.001)} + 1.37 \cdot 10^{-14} T_e^{-0.557} e^{-20.3/T_e}$
2	$e + H_2 \rightarrow 2H + e$	$1.54 \cdot 10^{-14} T_e^{0.06} e^{8.63/T_e} + 1.11 \cdot 10^{-13} T_e^{-0.813} e^{-13.4/T_e}$
3	$e + H_2(v = 0-14) \rightarrow H + H^-$	$1.972 \sigma_v^{(0)} \frac{T_e^{1/2}}{1+T_e/E_0} e^{-\frac{\Delta E_{th,v}}{T_e}} \left[\frac{\lvert E_{th,v}\rvert}{T_e} + \frac{1}{1+T_e/E_0}\right] \cdot (10^{-14})$
4	$e + H \rightarrow H^+ + 2e$	$k_4 = 9.74 \cdot 10^{-15} T_e^{-0.174} e^{-14.3/(T_e-0.001)} + 6.35 \cdot 10^{-15} T_e^{0.433} e^{-16.4/T_e}$
5	$H + H_2^+ \rightarrow H_2 + H^+$	$k_4 = 1.54 \cdot 10^{-14} T_e^{-0.859} e^{-4.61/(T_i-0.786)} + 1.64 \cdot 10^{-15} T_i^{-0.353} e^{-0.258/T_i}$
6	$e + H_2^+ \rightarrow H + H^+ + e$	$3.50 \cdot 10^{-13} T_e^{-1.25} e^{-3.19/(T_e-0.008)} + 1.77 \cdot 10^{-13} T_e^{-0.0924} e^{-3.04/T_e}$
7	$e + H_3^+ \rightarrow H_2^+ + H^-$	$1.93 \cdot 10^{-15} T_e^{-1.07} e^{-6.26/(T_e+0.131)} + 5.35 \cdot 10^{-17} T_e^{-0.371} e^{-2.07/T_e}$
8	$H_2 + H_2^+ \rightarrow H + H_3^+$	$6.29 \cdot 10^{-15} T_i^{-1.46} e^{-2.22/(T_i+0.356)} + 2.71 \cdot 10^{-16} T_e^{-1.30} e^{-0.317/T_i}$
9	$H^+ + H^- \rightarrow 2H$	$4.46 \cdot 10^{-14} T_i^{-0.281} + 1.26 \cdot 10^{-14} e^{-1.96/T_i}$
10	$H_2^+ + H^- \rightarrow H_2 + H$	$2.23 \cdot 10^{-14} T_i^{0.425} + 8.93 \cdot 10^{-14} T_i^{-0.261}$
11	$H_3^+ + H^- \rightarrow 0.5H_2 + 3H$	$1.70 \cdot 10^{-14} T_i^{0.313} + 5.75 \cdot 10^{-14} T_i^{-0.288}$
12	$e + H^- \rightarrow H + 2e$	$4.58 \cdot 10^{-13} T_e^{0.287} e^{-4.41/(T_e+0.117)} + 2.71 \cdot 10^{-14} T_e^{0.62} e^{-1.82/T_e}$
13	$e + H_3^+ \rightarrow 2H + H^+ + e$	$2.69 \cdot 10^{-13} T_e^{-0.245} e^{-15.6/(T_e+0.003)} + 1.01 \cdot 10^{-12} T_e^{-0.464} e^{-26.8/T_e}$
14	$H_2 + H^+ \rightarrow H_3^+ + h\nu$	$1.63 \cdot 10^{21}$
15	$e + H_2^+ \rightarrow 2H$	$2.29 \cdot 10^{-14} T_e^{-0.571} + 3.31 \cdot 10^{-15} T_e^{-0.152 T_e}$
16	$e + H_3^+ \rightarrow 3H$	$3.36 \cdot 10^{-15} T_e^{-0.716} + 3.73 \cdot 10^{-14} T_e^{-0.67} e^{6.40/T_e}$
17	$e + H_3^+ \rightarrow H + H_2$	$2.03 \cdot 10^{-15} (T_e^{-0.189} + 0.040 T_e^{-1.49}) + 5.57 \cdot 10^{-14} T_e^{1.23} e^{-6.21/T_e}$
18	$H + H^- \rightarrow H_2 + e$	$2.16 \cdot 10^{-13} T_i^{-1.89} e^{-12.7/(T_i+1.17)} + 1.30 \cdot 10^{-15} T_i^{-0.418} e^{-0.192/T_i}$
19	$H_2 + H^- \rightarrow H + H_2 + e$	$1.62 \cdot 10^{-16} T_i^{0.417} e^{-6.47/(T_i+0.132)} + 5.70 \cdot 10^{-16} T_i^{0.550} e^{-2.19/T_i}$
20	$H + H^- \rightarrow 2H + e$	$3.81 \cdot 10^{-15} T_i^{0.280} e^{-3.76/(T_i+0.626)} + 4.55 \cdot 10^{-16} T_i^{0.603} e^{-0.375/T_i}$
21	$H_2 + H^+ \rightarrow H + H_2^+$	$5.54 \cdot 10^{-16} T_i^{-0.453} e^{-3.26/(T_i-0.001)} + 5.98 \cdot 10^{-18} T_i^{-2.88} e^{-0.310/T_i}$
22	$e + H \rightarrow H^- + h\nu$	$5.75 \cdot 10^{-20} (T_e^{-0.0285} - 0.94 T_e^{-0.05}) + 6.54 \cdot 10^{-19} T_e^{-5.18} e^{-72.4/T_e}$

TABLE II: Plasma reactions and reaction rates used for this fluid transport model.

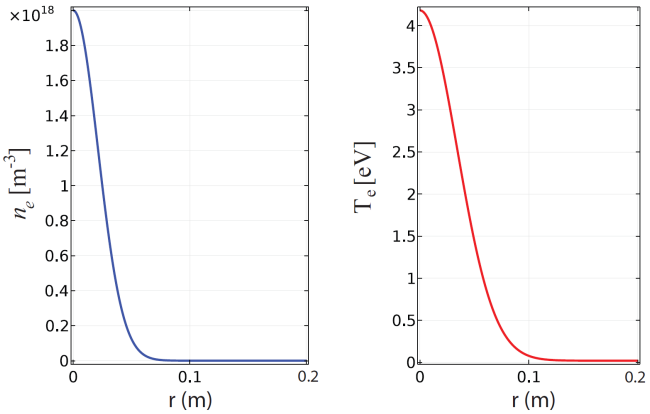

FIG. 1: Electron density and temperature radial profiles used as input in the model, obtained by fitting experimental data.[26] These profiles are representative for a hydrogen plasma discharge with 3 kW RF power, 0.3 Pa gas pressure at 1 m from the center of the antenna.

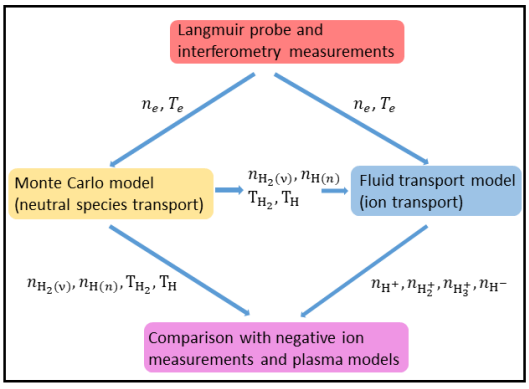

FIG. 2: Flow chart describing the coupling between the fluid and the Monte Carlo model.

as a reasonable approximation of the dissociative attachment reaction rate k_{DA}.[28] In this study, however, we use a Monte

Carlo model to estimate the radial density profiles of each rovibrational state of H_2 which are then inserted as input in the fluid part of the model.

IV. A MONTE CARLO (MC) MODEL TO DETERMINE NEUTRAL DENSITY PROFILES

In order to increase the self-consistency of the model, the plasma dynamics needs to be coupled with the neutral kinetics. In particular, the H_2 vibrational kinetics is important since the negative ion production is heavily dependent on the molecular vibrational distribution function (VDF). For this purpose, a Monte Carlo (MC) approach has been used to describe the dynamics and kinetics of the neutral gas particles (atoms and molecules) considering plasma (electron and ion species) as a fixed background with non-uniform density and temperature distributions (input of the plasma fluid model). This gas-plasma decoupling is a necessary hypothesis due to the very different plasma and gas kinetic time scales; the first in the microseconds, while the latter in the milliseconds ranges.
The MC model[29] is one-dimensional in the radial direction keeping the same geometrical reduction arguments used for the plasma fluid model, namely, the uniformity along the axial and the azimuthal direction, as mentioned in the introduction paragraph. The simulation starts with a uniform radial distribution of molecules (corresponding to a gas pressure $P_{gas} = 0.3\,\mathrm{Pa}$ and temperature $T_{H_2} = 300\,\mathrm{K}$); every time step a certain number of molecules is injected uniformly along the radial domain in order to keep the number of molecules fixed. This mimics numerically the continuous axial flow of molecules necessary to keep the gas pressure constant. Each particle contains information about its electronic (for atoms) and vibrational (for molecules) state. Only the fundamental electronic state of H_2 is taken into account. No information on rotational state is considered since the high ionization coefficient and the electron temperature involved guarantee a rotational equilibrium distribution. In the dissociative attachment reaction, the effect of the rotational excitation is smaller compared to that of the vibrational excitation.[30] The most relevant collisions with electrons and H^+ ions (the dominant ion species, see Sec. V) are considered through the use of state selective cross sections,[31–33] while neutral-neutral collisions are negligible due to the low pressure regime. The equations of motions of particles are solved and the heterogeneous surface processes are taken into account in the impact with the wall by using appropriate energy-dependent and state-dependent coefficients. The cross section of neutral/ion-surface processes involves a complex kinetic in which cross sections depend on neutral/ion and surface temperature.[34] For atoms, reflection and recombination coefficients,[35,36] while for molecules, relaxation and dissociation coefficients.[37,38] The gas subsystem reaches a steady state condition after 4 milliseconds, showing a global dissociation coefficient (Eq. 14) of $D_d = 0.103$. The radial averaged VDF is reported in Fig. 3 and shows the typical parabolic Treanor for the first 4 vibrational levels and hyperbolic plateau for ≥ 4, corresponding to a two-temperature distribution $T_{01} = 2000\,\mathrm{K}$ and $T_{07} = 7000\,\mathrm{K}$.

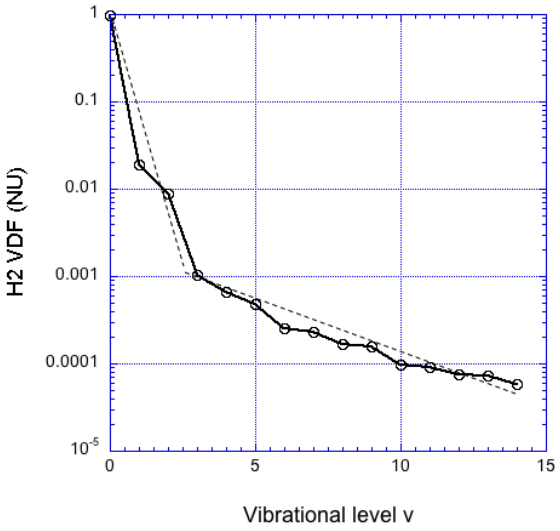

FIG. 3: Radial averaged $n_{H_2(v)}$ VDF (normalized to the $v = 0$ level density) as result of the MC model display a two-temperature distribution.

Once the n_H and n_{H_2} radial density profiles have been determined, the degrees of ionization and dissociation can be computed; these are shown in Fig. 4. The degree of ionization, defined as:

$$D_i = \frac{n_e}{n_H + n_{H_2}}, \tag{13}$$

is peaked at the center where it attains about 2%. The degree of dissociation, defined as:

$$D_d = \frac{n_H}{n_H + 2n_{H_2}}, \tag{14}$$

is slightly hollow at the center and around 10% across the vessel. The D_d (dissociation degree) well at the center of the plasma column is mainly due to a combination of central plasma heating and H transport towards the walls. H atoms produced by dissociation take about 2.2 eV each therefore, they are much hotter compared to the ~ 0.1 eV H_2 translation temperature.

V. TRANSPORT OF ION SPECIES

A. Ion density equilibrium and potential profiles

By solving the system of coupled equations Eq. (2), (3) and (4), the density of each ion species can be computed, as depicted in Fig. 5, together with the net source rate profiles (production - destruction) for H^+, H_2^+, H_3^+ and H^-. H^+, H_2^+

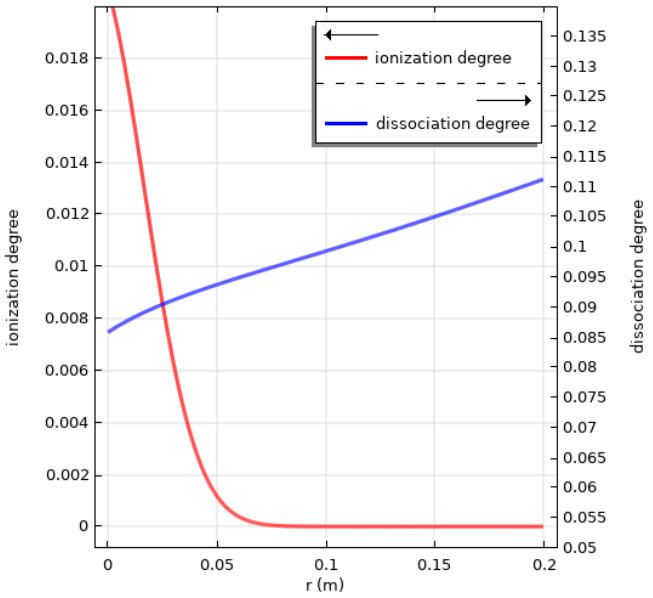

FIG. 4: Ionization and dissociation degree derived from the MC simulation.

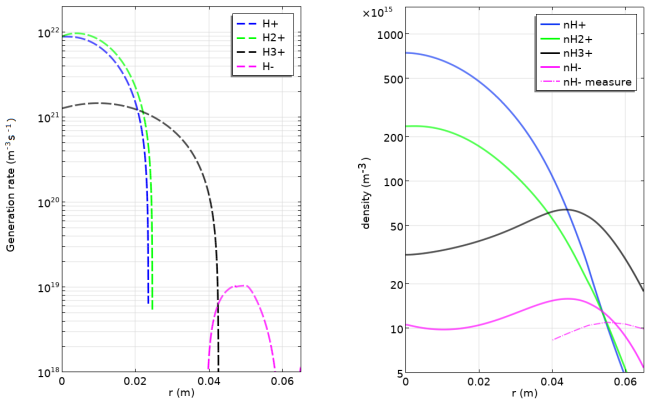

FIG. 5: Net generation rate (on the left) and density profiles (on the right) of ion species computed by the fluid model, including experimental n_{H^-} data.

show centrally peaked density profiles, while H_3^+ peaks on the edge. The H^- density profile also shows a shell-like structure, whose width and absolute value are comparable to measurements performed with laser-based diagnostics.[7] H^- net production takes place in a region of ≈ 1 cm width on the edge of the plasma column at ≈ 5 cm and H^- density peaks at ≈ 5 cm. This result suggests that transport plays an important role in the H^- density equilibrium profiles and a not negligible quantity is transported to the center of the plasma column. At the position of the H^- density peak, H_2^+ and H_3^+ densities are also comparable to that of H^+. This result shows that the plasma column is characterized by a hot and dense core region of ionising plasma dominated by H^+ surrounded by a halo of H_2^+ and H_3^+ recombining plasma. In the latter region, H^- are efficiently produced and can survive.

In Fig. 6 we show the computed profiles of the plasma po-

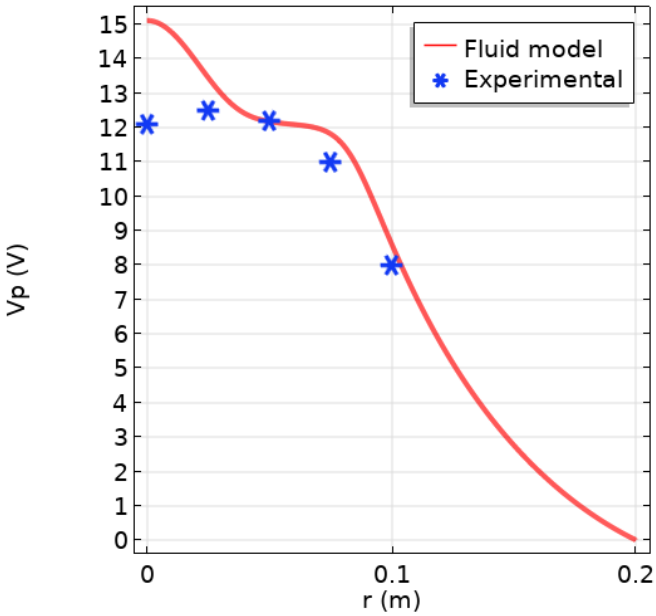

FIG. 6: Plasma potential calculated by the fluid model (dashed line) and experimental data (asterisks). Axial particle losses to walls are finely tuned so that the computed V_p matches the experimental points.[26]

tential which is self-consistently obtained by the resolution of Poisson's equation with the constraint of potential grounding on the wall and the boundary targets. The presence of electric forces arising from charge displacement guarantees the charge quasi-neutrality, so that an explicit charge conservation equation is not needed. Fig. 6 shows the computed plasma potential profile. It shows a central region with a small peak and a monotonic decay to the wall. The absolute peak value is sensitive to axial losses ($\Gamma_z(r)$), which are not self-consistently calculated. The axial losses are finely tuned to match the computed potential profile with the experimental V_p profile.[26] However, the absolute profile of plasma potential has only a weak influence on the computed plasma species profiles and transport. Since the plasma potential profile is strongly dependent on boundary conditions, a rigorous treatment would require to include the physics of the sheath, which goes beyond the scope of this model.

To have an insight of plasma species transport radially across the vessel section, it is instructive to plot the flux of different ions. Fig. 7 shows the absolute values of the flux for each plasma species across the radius. The arrows show the direction of the fluxes. H^+ and H_2^+ fluxes peak at about 2 cm from the center and are lost in a few cm due to volume destruction processes with background gas. H_3^+ are transported from the shell region up to the vessel wall. H^- are transported inward across the radius.

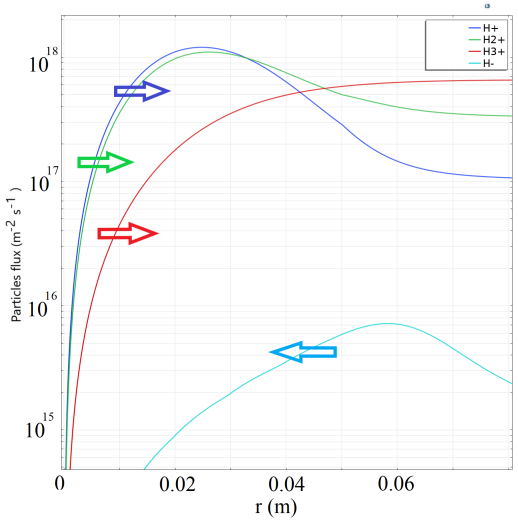

FIG. 7: Fluxes of ions across the radius. Positive ions are transported outwards, while H^- are transported inwards and destroyed by electron detachment and mutual neutralization with positive ions.

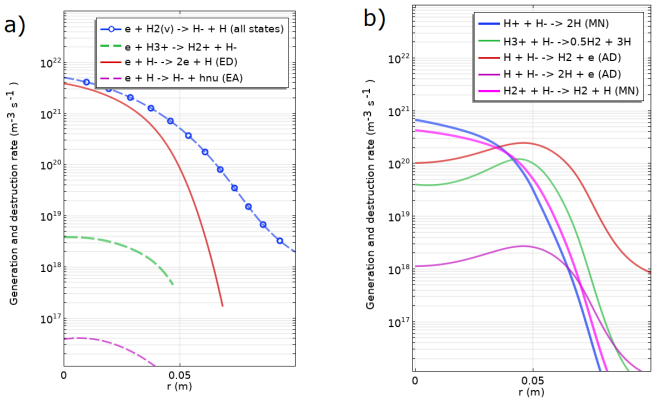

FIG. 8: Individual production (dotted lines) and destruction (continuous lines) processes of H^- along the radius induced by electrons, on the left, and by ions and neutrals, on the right. The dissociative attachment from ro-vibrationally excited H_2 is the dominant production process. In the plasma center, H^- is mainly detached by electron impact, while at the edge, mutual neutralization processes with positive ions and associative detachment are the main loss reactions.

B. Production and destruction mechanisms of H^-

Here we study each generation and loss mechanism of H^- to better understand volume production and destruction processes. In conventional negative ion sources for HNB injectors, the production of negative ions is achieved in two steps taking place in two different volumes: a region called *driver* where molecular hydrogen (or deuterium) is dissociated, and an expanding region with a caesiated surface where H/D atoms pick up electrons. In the case of a Cs-free negative ion source such as RAID, where negative ions are only produced in the plasma volume, it is interesting to study the contribution of production and destruction processes along the radial direction.

In Fig. 8 we show the individual reaction rates for H^- production (dashed lines) and destruction processes (solid lines) for electron collision reactions, on the left, and for reactions involving only heavy species, on the right. These profiles are obtained considering as input parameters the measured electron density and temperature profiles shown in Fig. 1. The dissociative attachment reaction ($e + H_2(v) \rightarrow H^- + H$) from H_2 ro-vibrational excited states, is the main contributor to negative ion production. The main destruction processes in the plasma center are the electron detachment ($e + H^- \rightarrow 2e + H$) and the mutual neutralization with H^+ ($H^+ + H^- \rightarrow 2H$), however, at the edge of the plasma column, where H^- density is peaked ($r \approx 5\,cm$), the most important destruction processes are the mutual neutralization with H_3^+ and H_2^+ ($H^- + H_3^+ \rightarrow 0.5H_2 + 3H$, $H^- + H_2^+ \rightarrow H_2 + H$) and the associative detachment ($H + H^- \rightarrow H_2 + e$). Thus, negative ions are mostly produced on the axis but are efficiently destroyed simultaneously by electron detachment. They mostly survive on the edge of the column because T_e is lower, where a net creation of H^- occurs as shown in Fig. 5 which gives the sum of all the production and destruction rates for H^-.

VI. DISCUSSION AND CONCLUSION

A 1.5D ion fluid model was developed to better understand ion transport and species reactions in a helicon hydrogen plasma. The method is based on the separation of a fluid treatment for ions and a Monte Carlo model for the neutrals. On the basis of electron density and temperature measurements, the neutral equilibrium density profiles as well as the density of H_2 in each vibrational excited state can be found. These values are used as input for the 1.5D fluid transport model. Because of the interest in volume negative ion production in RAID, it is helpful to investigate the interplay of production and destruction processes of H^-. We have compared the reaction rate profiles with the steady state equilibrium densities to understand how ions are transported observing that negative ions have a net production rate in a shell at the edge of the plasma column, from where they diffuse towards the axis. We observe that H^- are mainly destroyed in the plasma center by electron detachment and are mutually neutralized by H_2^+ and H_3^+ at the edge, close to the peak density position. Future possible developments on H^- volume production in helicon sources should focus on finding a correct balance among these competitive mechanisms to maximize the volume density of H^- close to the extraction region. Preliminary proof-of-principle negative ion extraction tests in a radial geometry have been recently carried out.[39]

A first envisaged step of this model would be the inclusion of the axial transport, which could be helpful to understand plasma composition in expanding plasmas, such as those produced in conventional negative ion sources for HNB injectors. An important improvement would consist in the inclu-

sion of a power balance equation and a power deposition profile of helicon waves to self-consistently calculate the electron density and temperature profiles. The inclusion of full helicon wave equations and the plasma formation calculated self-consistently would be a considerable leap requiring a 3D geometry, since helicon waves have a full 3D structure.[13]

ACKNOWLEDGMENTS

This work has been carried out within the framework of the EUROfusion Consortium and has received funding from the Euratom research and training programme 2014 - 2018 and 2019 - 2020 under grant agreement No 633053. The views and opinions expressed herein do not necessarily reflect those of the European Commission. This work was supported in part by the Swiss National Science Foundation.

BIBLIOGRAPHY

[1] R. S. Hemsworth *et al.*, New J. Phys, **19**, 025005 (2017).
[2] G. Serianni *et al.*, Nucl. Fusion **60**, 066025 (2020).
[3] D. Wünderlich, R. Riedl, M. Fröschle, U. Fantz, and B. Heinemann, Plasma **2021**, 172–182 (2021).
[4] G. Fubiani, L. Garrigues, G. Hagelaar, N. Kohen, and J. P. Boeuf, New J. Phys. **19**, 015002 (2017).
[5] G. J. M. Hagelaar and N. Oudini, Plasma Phys. Control. Fusion **53**, 124032 (2011).
[6] I. Furno, R. Agnello, U. Fantz, A. Howling, R. Jacquier, C. Marini, G. Plyushchev, P. Guittienne, and A. Simonin, EPJ Web of Conferences **157**, 03014 (2017).
[7] R. Agnello, S. Béchu, I. Furno, P. Guittienne, A. A. Howling, R. Jacquier, G. Plyushchev, M. Barbisan, R. Pasqualotto, Y. Andrebe, I. Morgal, and A. Simonin, Nucl. Fusion **60**, 026007 (2020).
[8] A. Pandey *et al.*, Rev. Sci. Instrum. **88**, 103509 (2017).
[9] A. Pandey *et al.*, Plasma Phys. Control. Fusion **61**, 065003 (2019).
[10] J. Santoso *et al.*, Phys. Plasmas **22**, 093513 (2015).
[11] J. Santoso *et al.*, Plasma Sources Sci. Technol. **27**, 10LT03 (2018).
[12] P. Guittienne, E. Chevalier, and C. Hollenstein, J. Appl. Phys. **98**, 083304 (2005).
[13] P. Guittienne *et al.*, Plasma Sources Sci. Technol. **30**, 075023 (2021).
[14] G. Fubiani *et al.*, Phys. Plasmasn **28**, 063503 (2021).
[15] S. Lishev, L. Schiesko, D. Wünderlich, C. Wimmer, and U. Fantz, Plasma Sources Sci. Technol. **27**, 125008 (2018).
[16] P. Ricci, F. D. Halpern, S. Jollie, J. Loizu, A. Mosetto, A. Fasoli, I. Furno, and C. Theiler, Plasma Phys. Control. Fusion **54**, 124047 (2012).
[17] R. Jacquier, R. Agnello, B. P. Duteil, P. Guittienne, A. Howling, G. Plyushchev, C. Marini, A. Simonin, I. Morgal, S. Bechu, and I. Furno, Fusion Engineering and design **146**, 1140–1144 (2019).
[18] F. F. Chen, *Plasma Physics and Controlled Fusion*, 2nd edition (Springer, 2006).
[19] R. M. Magee, M. Galante, E. Carr, G. Lusk, D. W. McCarren, and E. E. Scime, Phys. Plasmas **20**, 125311 (2013).
[20] M. A. Lieberman and A. J. Lichtenberg, 2nd edition (John Wiley and Sons, New York., 1994).
[21] COMSOL MULTIPHYSICS , Version 5.6.
[22] J. Santoso, Ph.D. thesis, The Australian National University (2018).
[23] S. Shinohara, N. Kaneda, and Y. Kawai, Thin Solid Films. **316**, 139–147 (1998).
[24] P. Chabert and N. Braithwaite, Cambridge University Press (Cambridge, 2011).
[25] R. K. Janev, D. Reiter, and U. Samm, *Collision Processes in Low-Temperature Hydrogen Plasmas* (2003).
[26] R. Agnello, *Negative Hydrogen Ions In a Helicon Plasma Source*, Ph.D. thesis, EPFL (2020).
[27] M. Bacal, Nucl. Fusion **46**, S250–S259 (2006).
[28] A. Pigarov and S. Krasheninnikov, Physics Letters A **222**, 251–257 (1996).
[29] F. Taccogna, R. Schneider, S. Longo, and M. Capitelli, Physics of plasmas **14**, 073503 (2007).
[30] J. Horáček *et al.*, Phys. Rev. Lett. A **70**, 052712 (2004).
[31] R. Celiberto, R. K. Janev, A. Laricchiuta, M. Capitelli, J. M. Wadehra, and D. E. Atems, New J. Phys. **18**, 125005 (2016).
[32] P. S. Krstic and D. R. Schultz, J. Phys. **B36**, 575–588 (2003).
[33] Hunter-Kuriyant, Proceedings of the Royal Society of London. Series A, Mathematical and Physical Sciences **353**, 575–588 (1977).
[34] A. Fridman, *Plasma Chemistry*, Cambridge University Press (New York, 2008).
[35] Y. H. Kim *et al.*, Chem. Phys. Lett. **314**, 1 (1999).
[36] M. Rutigliano, Plasma Sources Sci. Technol. **23**, 045016 (2014).
[37] G. D. Billing and M. Cacciatore, AIP Conf. Proc. **380**, 118 (1995).
[38] J. R. Hiskes and A. M. Karo, Appl. Phys. Lett. **54**, 508 (1989).
[39] F. Taccogna *et al.*, Eur. Phys. J. D **227**, 75 (2021).